ISSN (Print) : 0974-6846
Indian Journal of Science and Technology, *Vol 8(32), DOI: 10.17485/ijst/2015/v8i32/87491 , November 2015* ISSN (Online) : 0974-5645

By Wavelet based Fusion Directional Adaptive Interpolation Super Resolution Image Construction

S. Caroline Kirupa Shiny[1*] and R. Renita Rexy[2]

[1]Department of Electronics and Communication Engineering, Jerusalem College of Engineering, Chennai - 600100, Tamil Nadu, India; carolinesam88@gmail.com

[2]Department of Electronics and Communication Engineering, Bharath University, Chennai - 600073, Tamil Nadu, India; renitarexy.ece@bharathuniv.ac.in

Abstract

Super resolution is the process of recovering a high resolution image from multiple low resolution images of the same scene. This process consists of three steps: Image registration, Image fusion and Interpolation. Image registration is the first step in super resolution process in which the reference and sensed images are geometrically aligned. This alignment is done based on maximization of an appropriate similarity measure. The similarity measure used in this paper is Pearson correlation coefficient. Methods used for fusion are Discrete Wavelet Transform (DWT) based decomposition at one level and DWT based decomposition at 2 level. Interpolation is the final step in super resolution process. Various interpolation algorithms namely, nearest neighbour, bi-cubic, edge oriented interpolation, angular variation based interpolation and directional adaptive interpolation were applied to the images and are compared quantitatively. The overall performance of super resolution algorithms are compared using sharpness index metric.

Keywords: Image Registration, Pearson Correlation Coefficient, Sharpness Index, Sobel Operator

1. Introduction

In most electronic imaging applications, images with High Resolution (HR) are desired and often required. High Resolution means pixel density within an image is high, and therefore an HR image can offer more details that may be critical in various applications. Super resolution reconstruction[3] is the process of recovering a high resolution image from multiple low resolution images of the same scene. This process consists of three steps: image registration, fusion and interpolation.

Accurate image registration[7,12,13] is a crucial step in the super resolution process. Images captured by various sensors of the same scene may be oriented along different directions. Registration is the process of geometrically aligning the input images as in[13]. Image registration methods are classified into two main approaches: Intensity based methods and feature based methods as in[2].

Existing super-resolution fluorescence microscopes compromise acquisition speed to provide subdiffractive sample information. We report an analog implementation of structured illumination microscopy that enables Three-Dimensional (3D) super-resolution imaging with a lateral resolution of 145 nm and an axial resolution of 350 nm at acquisition speeds up to 100 Hz.

Image fusion[14] is the process of combining two or more images into a single image retaining important features from each. Image fusion is performed to integrate the information from the low resolution images, prior to the interpolation step as in[1]. The objective is to maintain the

* *Author for correspondence*

important information from the low-resolution images, which would not occur if the interpolation was carried out on the registered image directly.

The final step in the super-resolution process is the interpolation step[4]. It is a technique which estimates a new pixel from the surrounding pixels available in the low resolution image. Nearest neighbor and bi-cubic interpolation are the two conventional methods used for interpolation.

Section 2 describes the image registration algorithm, the image fusion algorithms are discussed in section 3 and the interpolation algorithms are presented in section 4. Super resolution algorithms are compared in section 5 and the conclusions are presented in section 6.

2. Image Registration

Image registration is done as in[8]. It is done by considering two low resolution images namely, *A* and *B*. These two images must be geometrically aligned prior to fusion step. Thus our aim is to calculate the coordinates of image *B* that corresponds to the origin of reference image *A*. Let the dimension of the low resolution images be $a \times b$. Let $w(i, j)$ represent a window with size $n \times n$ on image *A*. Let $g(i, j)$ represent the search area in image *B*. For both $w(i, j)$ and $g(i, j)$, the upper left corner is located at the origin of a global coordinate system[5,6].

Then it is clear that all the possible positions of the window $w(i, j)$ in the search area $g(i, j)$, takes values in the following set,

$$S = [0, N - 1] \text{ X } [0, M - 1] \tag{1}$$

where $N = a\text{-}n+1$ *and* $M = b\text{-}n+1$

Let $w1(i, j)$ be a window in the search area $g(i, j)$ that has the same size as that of w. The window $w1(i, j)$ is moved over the search area of image *B* along the *x* and *y* directions as an overlapping window. A condition is searched such that $w1(i, j)$ matches with $w(i, j)$. This matching is done based on maximization of an appropriate similarity measure. Images are registered by finding the coordinate position at which the value of the similarity measure is maximum. The size of the window used is 64×64. The similarity measure used is Pearson correlation coefficient.

Perason coefficient is calculated using (2).

$$r_{xy} = \left(\frac{\sum_{i=1}^{n}(x_i - \bar{x})(y_i - \bar{y})}{\sqrt{\sum_{i=1}^{n}(x_i - \bar{x})\sum_{i=1}^{n}(y_i - \bar{y})}} \right) \tag{2}$$

where x_i and y_i represents the gray scale values in matrix *A* and *B* respectively, $\bar{x}$ *and* $\bar{y}$ represents mean values of matrices *A* and *B* respectively and *n* represents the total number of values in matrix *A* or matrix *B*.

3. Image Fusion

Two techniques for performing image fusion namely, fusion using wavelet transforms at one level and two levels[1,11] are compared in the following sections.

3.1 Fusion using One Level Wavelet Transform

Step 1. Apply DWT decomposition (1 level) to input images, $f_1(m, n)$ and $f_2(m, n)$

Step 2. For each pixel of $LL_1^k(m,n)$ (i.e., approximation or low frequency sub band), identify 3×3 windows $CLH_1^k(m,n), CHL_1^k(m,n)$ *and* $CHH_1^k(m,n)$, centered at the corresponding pixels in $LH_1^k(m,n), HL_1^k(m,n)$ *and* $HH_1^k(m,n)$, sub-bands (i.e., detail or high-frequency sub bands), where k = 1, 2 and represents the images involved in fusion.

1. Find :

$$CA_1^k(m,n) = abs\{CLH_1^k(m,n)\} + abs\{CHL_1^k(m,n)\} + abs\{CHH_1^k(m,n)\}.$$

2. Find the mean $MA_1^k(m,n)$ and standard deviation $SA_1^k(m,n)$ *of* $CA_1^k(m,n)$ of as activity levels.

3. Fuse wavelet coefficients of LL_1 using the Fusion rule as follows.

$$F(m,n) = \begin{cases} LL_1^1(m,n); & \text{if } MA_1^1(m,n) > MA_1^2(m,n) \\ LL_1^2(m,n); & \text{if } MA_1^1(m,n) < MA_1^2(m,n) \\ & \text{and } SA_1^1(m,n) < SA_1^2(m,n) \\ \{LL_1^1(m,n) + LL_1^2(m,n)\}/2; & \text{otherwise} \end{cases} \tag{3}$$

Step 3. For each pixel of $LH_1^k(m,n)$, (i.e., high frequency sub band), find the standard deviation SD_1^k, over 3×3 windows, where k = 1, 2 represent the images involved in fusion. Fuse the wavelet coefficients of $LH_1^k(m,n)$, sub-band using the fusion rule as follows

$$F(m,n)=\begin{cases} LH_1^1(m,n); & \text{if}: SD_1^1(m,n) > SD_1^2(m,n) \\ LH_1^2(m,n); & \text{if}: SD_1^1(m,n) < SD_1^2(m,n) \\ \{LH_1^1(m,n)+LH_1^2(m,n)\}/2; & \text{otherwise} \end{cases} \quad (4)$$

Step 4. Repeat step 3 for other high frequency sub bands.

Step 5. Apply Inverse DWT to get the fused image.

3.2 Fusion using Two Level Wavelet Transform

The following steps are involved in the fusion of images using wavelet transform at two level.

Step 1. Apply DWT decomposition (1 level) to input images, $f_1(m, n)$ and $f_2(m, n)$.

Step 2. For each pixel of $LL_2^k(m,n)$, identify 3×3 windows $CLH_2^k(m,n), CHL_2^k(m,n)$ *and* $CHH_2^k(m,n)$, centered at the corresponding pixels in $LH_2^k(m,n), HL_2^k(m,n)$ *and* $HH_2^k(m,n)$, sub-bands, where k = 1, 2 and represents the images involved in fusion.

1. Find $CA_2^k(m,n) = abs\{CLH_2^k(m,n)\} + abs\{CHL_2^k(m,n)\} + abs\{CHH_2^k(m,n)\}$.
2. Find the mean $MA_2^k(m,n)$ and standard deviation $SA_2^k(m,n)$ *of* $CA_2^k(m,n)$ as activity levels.
3. Fuse wavelet coefficients of LL_2 using the Fusion rule as follows

$$F(m,n)=\begin{cases} LL_2^1(m,n); & \text{if } MA_2^1(m,n) > MA_2^2(m,n) \\ LL_2^2(m,n); & \text{if } MA_2^1(m,n) < MA_2^2(m,n) \\ & \quad \text{and } SA_2^1(m,n) < SA_2^2(m,n) \\ \{LL_2^1(m,n)+LL_2^2(m,n)\}/2; & \text{otherwise} \end{cases} \quad (5)$$

Step 3. For each pixel of $LH_m^k(m,n)$, (i.e., high frequency sub band), find the standard deviation SD_m^k, over 3×3 windows, where k = 1, 2 represent the images involved in fusion and m = 1, 2 represents the levels of DWT decomposition. Fuse the wavelet coefficients of $LH_m^k(m,n)$, sub-band using the fusion rule as follows

$$F(m,n)=\begin{cases} LH_m^1(m,n); & \text{if}: SD_m^1(m,n) > SD_m^2(m,n) \\ LH_m^2(m,n); & \text{if}: SD_m^1(m,n) < SD_m^2(m,n) \\ \{LH_m^1(m,n)+LH_m^2(m,n)\}/2; & \text{otherwise} \end{cases} \quad (6)$$

Step 4. Repeat step 3 for other high frequency sub bands.

Step 5. Apply Inverse DWT to get the fused image.

3.3 Comparison of Image Fusion Algorithms

Mutual Information[11] (MI) is used for measuring and comparing the fusion performance. Several test images were fused using the two fusion algorithms and they were compared quantitatively[15,16].

The higher the value of this parameter, the greater is the efficiency of the fusion algorithm being used.

Mutual information calculated for all the two fusion algorithms are shown in Table 1. From this table it is clear that for several test images the mutual information using one level DWT is the highest.

Table 1. Comparison of mutual information

Test Images	1 level DWT	2 level DWT
Child	5.889	5.775
Lena	4.016	3.946
Caps	6.283	6.201
Bike	5.592	4.387

4. Directional Adaptive Interpolation

Image interpolation based on cubic convolution was given by D. Zhou et al. in[13] in which the edge detection is done based on a preset threshold value. In the proposed method edge detection is done using Sobel operator. The Sobel operator performs a 2-D spatial gradient measurement on an image and so emphasizes regions of high spatial frequency that correspond to edges. Initially zeros are inserted after every row and column and Sobel operator is applied. To the output of Sobel operator a window of size 5×5 is moved and mean value of the window is calculated. If the mean value is greater than zero, the pixel corresponding to the centre position of the window is classified as edge pixel and if mean is equal to zero, it is classified as a smooth pixel[17]. Let P be the image to be interpolated. Compute matrix Q using matrix P, such that,

$$Q(2i, 2j) = P(i, j) \quad (7)$$

In this method, interpolation is performed in two steps. In the first step we compute the 'b' pixels, and then the 'a' pixels in the second step[10]. The 'b' pixels correspond to the pixels at $Q(i, j)$ where $(i+j)$ is even and 'a' pixels correspond to the pixels at $Q(i, j)$ where $(i+j)$

is odd. The 'a' and 'b' pixels are shown in Figure 1. The 'b' pixels have their 4 interpolation neighbours already known[18]. The 'a' pixels will have 4 neighbours only after 'b' pixels have been determined.

4.1 Interpolation of Diagonal and Axial Pixels

For each 'b' pixel to be interpolated, its neighboring pixels covered by a 7×7 window are projected along two different angular orientations i.e., along 45° and 135°. For every orientation, gradients are calculated using (8) and (9).

$$G_1 = \sum_{m=3,\pm1}\sum_{n=3,\pm1} \left|I(i+m, j-n) - I(i+m-2, j-n+2)\right| \quad (8)$$

(45° *diagonal*)

$$G_2 = \sum_{m=3,\pm1}\sum_{n=3,\pm1} \left|I(i+m, j+n) - I(i+m-2, j-n-2)\right| \quad (9)$$

(135° *diagonal*)

x_1	a	x_3	a	x_5	a	x_7
a	b	a	b	a	b	a
x_{15}	a	x_{17}	a	x_{19}	a	x_{21}
a	b	a	b	a	b	a
x_{29}	a	x_{31}	a	x_{33}	a	x_{35}
a	b	a	b	a	b	a
x_{43}	a	x_{45}	a	x_{47}	a	x_{49}

Figure 1. 7X7 matrix representing diagonal pixels 'b' and axial pixels 'a' to be interpolated.

After the estimation of gradients the direction of the edge is calculated for edge pixels using (10) and the value of 'b' pixel is calculated using (11).

$$\begin{cases} if \quad G_1/G_2 > G_2/G_1; pixel\,is\,on\,135° edge \\ if \quad G_2/G_1 > G_1/G_2; pixel\,is\,on\,45° edge \end{cases} \quad (10)$$

$$b = \begin{cases} \dfrac{-x_7 + 9x_{19} + 9x_{31} - x_{43}}{16} & ;45° edge\ pixel \\ \dfrac{-x_1 + 9x_{17} + 9x_{33} - x_{49}}{16} & ;135° edge\ pixel \end{cases} \quad (11)$$

For the interpolation of smooth pixels, the following equation is used.

$$b = (w_1 p_1 + w_2 p_2)/(w_1 + w_2)$$

Where,

$$p_1 = \frac{-x_7 + 9x_{19} + 9x_{31} - x_{43}}{16}$$

$$p_2 = \frac{-x_1 + 9x_{17} + 9x_{33} - x_{49}}{16} \quad (12)$$

$$w_1 = \frac{1}{1+G_1^k}$$

$$w_2 = \frac{1}{1+G_2^k}$$

After the interpolation of 'b' pixels the 'a' pixels are interpolated using the same procedure with its axial neighbors.

4.2 Comparison of Interpolation Algorithms

Standard test images of size 256×256 were interpolated using various interpolation algorithms and they were compared visually and quantitatively[19]. For quantitative analysis, correlation coefficient was calculated for the interpolated image and standard test images of size 512×512 using (2). Correlation coefficient value depicts the similarity between two input images. It has a maximum value of 1, when both the input images are exactly similar[20]. The values of correlation coefficient for various interpolation algorithms are shown in Table 2. This table depicts that correlation coefficient value computed for various images using directional adaptive interpolation algorithm is highest. Hence directional adaptive interpolation algorithm out performs other algorithms.

Table 2. Comparison of correlation coefficient for various interpolation algorithms

Test image	Bi-cubic	Edge Oriented	Adaptive directional
Child	0.9714	0.9838	0.9910
Lena	0.9709	0.9813	0.98946
Caps	0.9736	0.9897	0.9969
Bike	0.9506	0.9626	0.9758

5. Comparison of Super Resolution Algorithms

To assess the quality of the final super resolution image

(a) (b) (c)

Figure 2. Interpolation results for house image obtained with. **(a)** Bicubic interpolation. **(b)** Edge directed. **(c)** Adaptive directional interpolation.

(a) (b) (c)

Figure 3. Interpolation results for light house image obtained with. **(a)** Bicubic interpolation. **(b)** Edge directed. **(c)** Adaptive directional interpolation.

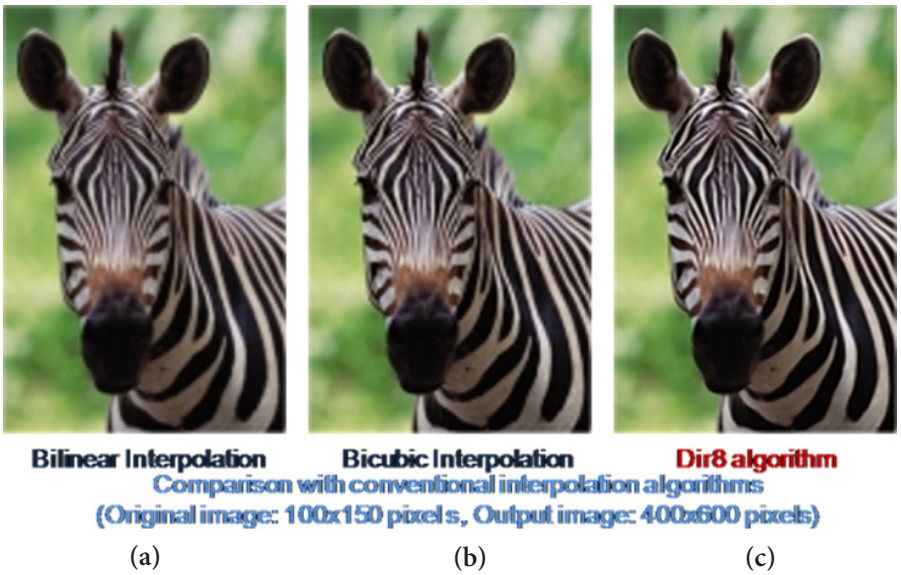

(a) (b) (c)

Figure 4. Comparision with conventional interpolation algorithms (Orginal image: 100x150 pixels, output image: 400x600 pixels). (a) Biliniar interpolation. (b) Bicubic interpolation. (c) Dir8 algorithm.

Table 3. Quantitative comparison of super resolution process

Methods	Sharpness Index			
	Flower image	Leaf image	Paper image	Plane image
2 Level DWT fusion with Edge directed interpolation	1104884	831290	2429894	214646
2 Level DWT fusion with adaptive directional interpolation	1123564	840889	2447438	216992
1 Level DWT fusion with Edge directed interpolation	1137896	874495	2650277	228361
1 Level DWT fusion with adaptive directional interpolation	1335084	979007	2909629	237054

sharpness index, M is used. Sharpness index is calculated using (13)

$$M = \sum_{x=0}^{n-1}\sum_{y=0}^{m-1}\|L(x,y)\| \quad (13)$$

where n×m is the size of the image and $L(x, y)$ is the output of the Laplacian filter, whose input is the pixel (x, y). The sharper the image, the larger will be the value of sharpness index[21]. Super resolution images obtained using different interpolation algorithms are shown in Figures 2 and 3.

6. Conclusion

It has been found from Table 3 that super resolution images constructed using Pearsons correlation coefficient based registration, 1 Level DWT based fusion and adaptive directional interpolation produces best results with reduced computational complexity.

7. References

1. Kimio T, Natarajan G, Hideki A, Taichi K, Nanao K. Higher involvement of subtelomere regions for chromosome rearrangements in leukemia and lymphoma and in irradiated leukemic cell line. Indian Journal of Science and Technology. 2012 Apr; 5(1):1801–11.
2. Cunningham CH. A laboratory guide in virology. 6th ed. Minnesota: Burgess Publication Company; 1973.
3. Sathishkumar E, Varatharajan M. Microbiology of Indian desert. In: Sen DN, editor. Ecology and Vegetation of Indian Desert. India: Agro Botanical Publishers; 1990. p. 83–105.
4. Varatharajan M, Rao BS, Anjaria KB, Unny VKP, Thyagarajan S. Radiotoxicity of sulfur-35. Proceedings of 10th NSRP; India. 1993. p. 257–8.
5. 01 Jan 2015. Available from: http://www.indjst.org/index.php/vision
6. Arivazhagan S, Ganesan L, Kumar TGS. A modified statistical approach for image fusion using wavelet transform. Signal, Image and Video Processing. 2009; 3:137–44.
7. Barbara Z, Flusser J. Image registration methods: A survey. 2003; 2:977–100.
8. Langeswaran K, Revathy R, Kumar SG, Vijayaprakash S, Balasubramanian MP. Kaempferol ameliorates Aflatoxin B1 (AFB1) induced hepatocellular carcinoma through modifying metabolizing enzymes, membrane bound ATPases and mitochondrial TCA cycle enzymes. Asian Pacific Journal of Tropical Biomedicine. 2012; 2(S3):S1653–9. ISSN: 2221-1691.
9. Glasner D, Bagon S, Irani M. Super-resolution from a single image. Int conf; Kyoto: Japan. 2009 Oct.
10. El-Khamy SE, Hadhoud MM, Dessouky MI, Salam BM, Abd El Samie FE. Efficient implementation of image interpolation as an inverse problem. Digital Signal Processing. 2005; 15(2):137–52.
11. Rajendran S, Muthupalani RS, Ramanathan A. Lack of Ring Finger Domain (RFD) mutations of the c-Cbl gene in oral squamous cell carcinomas in Chennai, India. Asian Pacific Journal of Cancer Prevention. 2013; 14(2):1073–5. ISSN: 1513-7368.
12. Maes F, Vandermeulen D, Suetens P. Medical image registration using mutual information. Proc of IEEE. 2003 Oct; 91(10):1699–722.
13. Nasir H, Stankovic V, Marshall S. Singular value decomposition based fusion for super-resolution image reconstruction. Digital Signal Processing. 2011; 27(2):180–91.
14. Anbazhagan R, Satheesh B, Gopalakrishnan K. Mathematical modeling and simulation of modern cars in the role of stability analysis. Indian Journal of Science and Technology. 2013; 6(S5):4633–41. ISSN: 0974-6846.
15. Huang TS, Tsai RY. Multi-frame image restoration and registration. Adv Comput Vis Image Process. 1984; 1:317–39.
16. Karybali IG, Psarakis EZ, Berberidis K, Evangelidis GD. An efficient spatial domain technique for subpixel image registration. Signal Processing: Image Communication. 2008; 23(9):711–24.
17. Menon R, Kiran CM. Concomitant presentation of alopecia areata in siblings: A rare occurrence. International Journal of Trichology. 2012; 4(2):86–8. ISSN: 0974-7753.
18. Zhou D, Shen X, Dong W. Image zooming using directional cubic interpolation. Proceedings of IET image processing. 2010; 6(6):627–34.
19. Chen M-J, Huang C-H, Lee W-L. A fast edge-oriented algorithm for image interpolation. Image and Vision Computing. 2005; 23(9):791–8.
20. Roshni VS. Mutual information based registration and region based wavelet fusion of images. IEEE Proceedings Conf of Computer Vision Graphics and Image Processing; Bhubaneswar. 2008 Dec 16-19. p. 606–13.
21. Muruganantham S, Srivastha PK, Khanaa. Object based

middleware for grid computing. Journal of Computer Science. 2010; 6(3):336–40. ISSN: 1552-6607.
22. Tian Q, Huhns MN. Algorithm for subpixel registration. Computer Vision, Graphics, Image Proc. 1986; 35(2):220–33.
23. Du Q, Chen L. An image registration method based on wavelet transformation. Proceedings of Computer, Mechatronics, Control and Electronic Engineering (CMCE) International Conference; Changchun. 2010 Aug 24-26. p. 158–60.
24. Tang J. A contrast based image fusion technique in the DCT domain. Digital Signal Processing. 2004; 14(3):218–26.
25. Li X, Orchard T. New edge-directed interpolation. IEEE Transactions on Image Processing. 2001; 10(10):1521–7.
26. Edge-directed interpolation. Available from: http://chiranjivi.tripod.com/EDITut.html